Atmósfera 34(4), 503-515 (2021)
https://doi.org/10.20937/ATM.52840

SHORT COMMUNICATION

A rare winter thunderstorm event near Hong Kong

Pak Wai CHAN[1]*, Kai Kwong HON[1] and Qiusheng LI[2]

[1]*Hong Kong Observatory, 134A Nathan Road, Kowloon, Hong Kong, China.*
[2]*Department of Architecture and Civil Engineering, City University of Hong Kong, Tat Chee Avenue, Kowloon, Hong Kong, China.*
*Corresponding author: email: pwchan@hko.gov.hk

Received: February 25, 2020; accepted: July 11, 2020

RESUMEN

En este trabajo se documenta una inusual tormenta eléctrica de verano ocurrida cerca de Hong Kong. La presencia de este fenómeno fue confirmada mediante observación por uno de los autores y por sistemas de información de localización de rayos, tanto locales como globales. Esta tormenta se desarrolló sobre el sistema frontal de nubes asociado con el monzón de invierno; sin embargo, las mediciones de altitud no mostraron condiciones termodinámicas favorables para la ocurrencia de una tormenta eléctrica. La energía potencial convectiva disponible no pudo determinarse en la troposfera inferior fría y seca. Sólo había una capa más húmeda en la troposfera media. El meteorólogo no pudo anticipar la aparición de truenos y relámpagos; no obstante, algunas condiciones pudieron haber cambiado dinámicamente y estos cambios podrían haber sugerido la posibilidad de una tormenta eléctrica. Por ejemplo, se pudieron identificar ondas en la troposfera media y en la troposfera baja se ubicó un amplio sistema de baja presión. Asimismo, se observó una onda integrada de vapor de alto nivel. Este trabajo busca servir a los meteorólogos como referencia útil para valorar la posibilidad de que ocurran tormentas eléctricas en latitudes subtropicales durante el invierno, asociadas con sistemas frontales de nubes.

ABSTRACT

A rare winter thunderstorm event near Hong Kong is documented in this paper. The thunderstorm occurrence was confirmed by the observation of one of the authors and lightning location information systems (both regional and global). It developed over the frontal cloud band associated with the winter monsoon. Observing the upper air measurements, however, the thermodynamic conditions did not seem favorable to the occurrence of the thunderstorm. The convective available potential energy could not be determined in the cool and dry lower troposphere. There was only a moister layer in the middle troposphere. The weather forecaster did not anticipate the occurrence of thunder and lightning. However, some features could have changed dynamically, which suggested the possibility that a thunderstorm would take place. For instance, waves could be identified in the middle troposphere and a broad troughing flow could be analyzed in the lower troposphere. The integrated wave vapor was also of a rather high level. It is hoped that this paper can serve as a useful reference for forecasters in assessing the possibility of thunderstorms occurring during winter over subtropical latitudes in association with frontal cloud bands.

Keywords: winter thunderstorm, satellite winds, dual pole radar, NWP simulation.

1. Introduction

Thunderstorms usually occur in Hong Kong during the summer, being rather rare during winter. According to the records of weather observers at the Hong Kong Observatory (HKO) headquarters, the climatological number of thunderstorm days in January for each year from 1947 to 2019 was 0.16 (HKO, 2020). It would be useful to document the meteorological conditions in which thunderstorms take place in or around the Hong Kong territory during January, with the aim of providing useful reference to weather forecasters for the identification of possible thunderstorms occurring during this season, when discharging their day-to-day operational forecasting duties.

A thunderstorm occurred at about 40 to 50 km to the southeast of Hong Kong during the morning of January 27, 2020. As could be seen in subsequent analysis, this thunderstorm was unexpected for one reason: it was not furthered by the thermodynamic conditions of the atmosphere (i.e., the various instability indices recorded by the upper air sounding systems were not conductive to the development of a thunderstorm). It is interesting to document this thunderstorm case for future reference. This paper also tries to summarize the atmospheric conditions that may have contributed to the occurrence of the thunderstorm. Such observations can serve as useful references to aid weather forecasters in their future assessment of the possibility of thunderstorms occurying near Hong Kong.

2. Data and analysis methodology

2.1 Surface-based meteorological observations

Weather radars are the major analysis tools of this paper. There are five microwave weather surveillance radars in Hong Kong. In the present analysis, two of them will be used: the long-range (512 km), S-band, dual polarization radar on the top of Tate's Cairn mountain (about 500 masl [Kong and Chan, 2018]); and the C-band terminal doppler weather radar (TDWR) at Brother's Point (Tse et al., 2019).

The S-band radar performs a volume scan every 6 min with a total of 11 elevation angles ranging between 0 to 34º from the horizontal. Apart from the conventional reflectivity and Doppler velocity, it is able to classify the nature of hydrometeors based on dual polarization parameters. The hydrometeor classification has a radial resolution of 150 m and an azimuthal resolution of 1º. For products presented in Cartesian coordinates, the finest resolution would be around 150 × 150 m per pixel. The algorithm currently in use at HKO is supplied by the radar manufacturer and based on Liu and Chandrasekhar (2000) with local adaptations. On the other hand, the C-band TDWR mainly focuses on the airport area of Hong Kong to provide windshear alerts. On top of dedicated sector scans covering the airport area with high revisiting frequency, it performs a 5º plan position indicator (PPI) scan at intervals of approximately 5 min with a range up to about 90 km as a backup for the S-band radar in long-range measurements. However, it should be noted that these PPI scans are affected by beam blockage over parts of the northern and eastern quadrants due to the TDWR's low construction height (by design) as compared to scans at the mountainous terrain in other parts of Hong Kong, measuring up to about 900 m.

Another important tool for lightning observation is the lightning location information system (LLIS). The HKO collaborates with the Guangdong Meteorological Bureau and the Macao Meteorological and Geophysical Bureau in operating a network of lightning sensors for detection over the south China coast and adjacent waters. Details of the LIIS can be found in Lee (2018). Starting from late 2016, the Observatory also receives near real-time global lightning location information (GLD360) from a service provider. Technical details of the GLD360 data set can be found in the manufacturer's website (https://www.vaisala.com/en/products/data-subscriptions-and-reports/data-sets/gld360). Both networks are able to detect cloud-ground (C-G) and cloud-cloud (C-C) lightning strikes (GLD360 data set began providing a differentiation of C-C and C-G strikes since early 2019). A comparison between the detection performance of the two data sources over the south China coastal areas can be found in Chiu and Lee (2019).

In order to observe the upper air atmospheric conditions, the Observatory operates a number of equipment, the first being the conventional radiosonde ascent, which is released at King's Park in the city center. The ascent is made twice a day, namely at 00:00 and 12:00 UTC (Hong Kong time = UTC

+ 8 h). It measures temperature, dew point, pressure and atmospheric winds, providing raw data at an observation frequency up to 2 Hz. Remote sensing meteorological instruments are also put into operation, one of which is a boundary layer type, vertically pointing radar wind profiler at the city center that measures the three components of the wind up to about 9 km above mean sea level (Chan and Yeung, 2003). There is also a ground-based microwave radiometer at King's Park, which provides temperature and dew point profiles up to 10 km above mean sea level (Chan, 2009). The retrieval algorithm used by the radiometer is described and detailed in Chan (2010). The radiosonde ascent and microwave radiometer data, such as K-index and convective available potential energy (CAPE), are used to calculate instability indices of the atmosphere, which could be useful indicators for the occurrence of thunderstorms in Hong Kong (Chan and Hon, 2011).

2.2 Satellite-based meteorological observations

To support daily forecasting operations, HKO receives real-time observation data from Himawari-8, a next-generation meteorological satellite of the Japan Meteorological Agency. Ranging from a central wavelength of 0.47-13.3 μm, the Advanced Himawari Imager on Himawari-8 operates at 16 frequency bands and covers both the infrared and visible spectra (Murata et al., 2015). HKO also operates satellite-based a regional nowcasting system (HKO, 2019) based on a locally adapted version of the EUMETSAT satellite application facility for Nowcasting and Very Short Range Forecasting (NWC SAF) (Derrien and Le Gléau, 2005). Various satellite analysis and nowcasting products generate real-time data including cloud type, cloud top height and derived winds.

2.3 Numerical weather prediction model

In section 4 we will inspect the performance of the AAMC-WRF model, which is a large-domain implementation of the Weather Research and Forecast (WRF) model (Skamarock and Klemp, 2007) at 10-km resolution developed by HKO to support regional aviation weather prediction. The configuration of the AAMC-WRF model follows Hon (2020). In essence, the forecast domain contains 1251 × 1101 grid points horizontally, spanning the region (20º S-60º N, 45º-160º E) and using the Mercator projection with 42 eta levels vertically. Version 3.9.1 of the WRF source code is used. At the time of writing this paper, the model followed a schedule of four runs per day (initialized at 00:00, 06:00, 12:00 and 18:00 UTC) and up to T + 48 h. Boundary conditions were provided by the latest available National Centers for Environmental Prediction-Global Forecasting System (NCEP GFS) output at 0.5º horizontal resolution. Initial conditions were provided by a 3DVAR analysis of surface and upper-air observations from the Global Telecommunication System (GTS) based on first guess fields from the latest available NCEP GFS output at 0.25º horizontal resolution. Key model configurations included were the WRF Double Moment 6-Class (WDM6) scheme for microphysics (Lim and Hong, 2010); the RRTMG schemes for short- and long-wave radiation (Iacono et al., 2008); the Noah land surface model (Niu et al 2011); the YSU planetary boundary layer scheme (Shin et al., 2013), and the modified Tiedtke scheme for cumulus convection (Zhang et al., 2011).

To support various weather forecasting functions at HKO, forecasts fields from the AAMC-WRF model are generated at 1-h intervals. In addition to conventional surface and upper-air parameters including sea level pressure, precipitation, winds, temperature, relative humidity and more, simulated infrared radiances following Hon (2018) and simulated radar reflectivity are also computed as routine products to facilitate direct visual comparison with remote sensing observations by weather forecasters in an operational setting.

3. Analysis of the event

3.1 Synoptic conditions

The thunderstorm event occurred at about 09:20 LT on January 27, 2020. Thunder was heard at the location of one of the authors in the city center. Meanwhile, the northeast monsoon was affecting mainland China up to the northern part of South China Sea (Fig. 1).

The meteorological satellite imagery showed that there were convective clouds just to the southeast of Hong Kong (Fig. 2a). The cloud top was analyzed to be about 8000 masl (Fig. 2b). Integrated water vapor reached 2-3 kg m^{-2} (Fig. 2c), which is a high value and showed there was abundant of moisture favorable to the development of convective clouds.

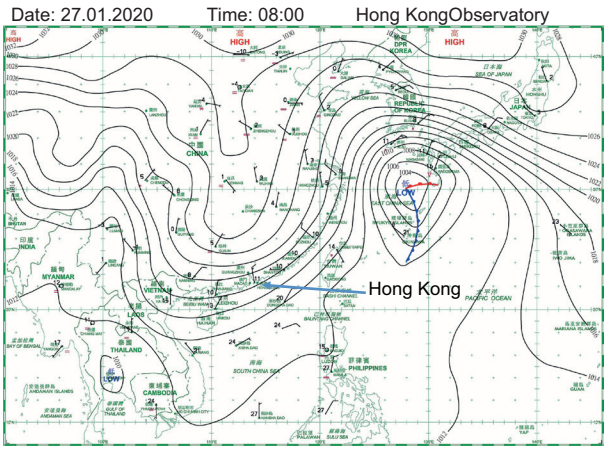

Fig. 1. Surface isobaric chart during the morning (00:00 UTC) on January 27, 2020.

Regarding cloud drift winds, there was a trough over the south China coastal area at around the 800 to 1000 hPa layers (Fig. 3a), namely northerly winds over the coast and inland areas, and westerly winds over the coastal waters. In the middle troposphere (600 to 800 hPa) (Fig. 3b) there was a southwesterly jet over south China coastal waters. Short waves could be found in the jet, which might as well trigger a deep convection. There may be gravity waves in the frontal clouds associated with the northeast monsoon over southern China and the south China coastal waters.

3.2 Local conditions

From the radarscope, intense radar echo (about 47 dBZ) with lightning strikes from LLIS was observed

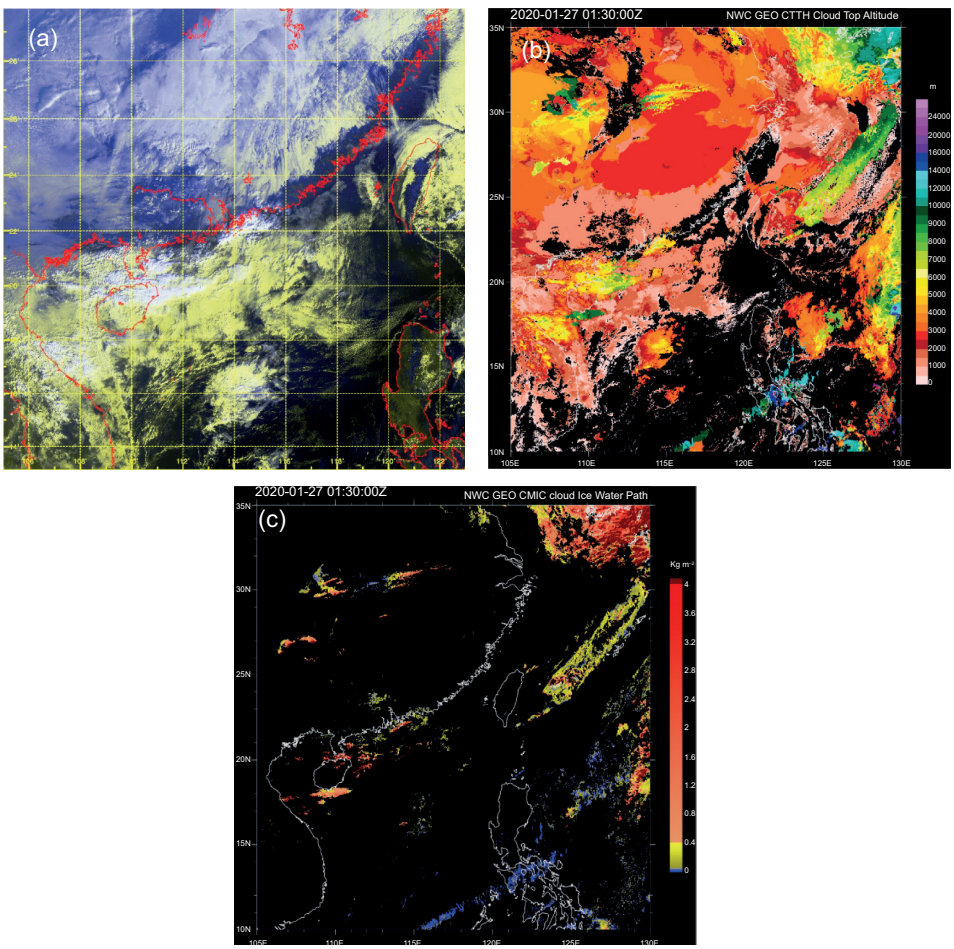

Fig. 2. Meteorological satellite images: (a) false color image, (b) cloud top height, and (c) integrated water vapor amount. The scales are given on the right side of (b) and (c).

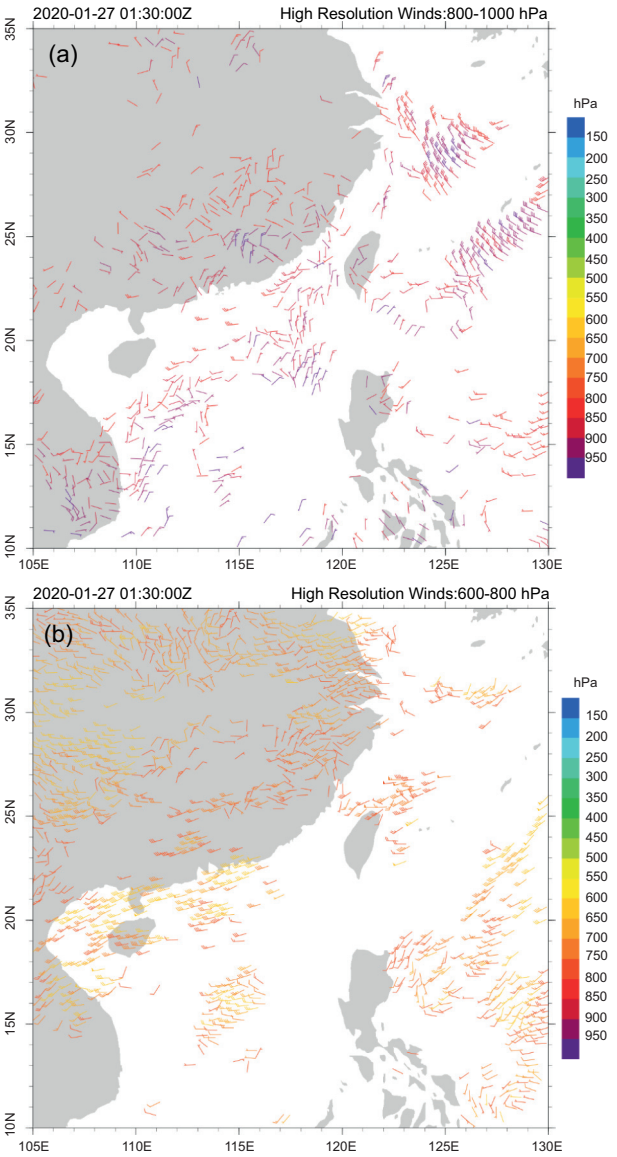

Fig. 3. Satellite derived winds for (a) lower troposphere and (b) middle troposphere.

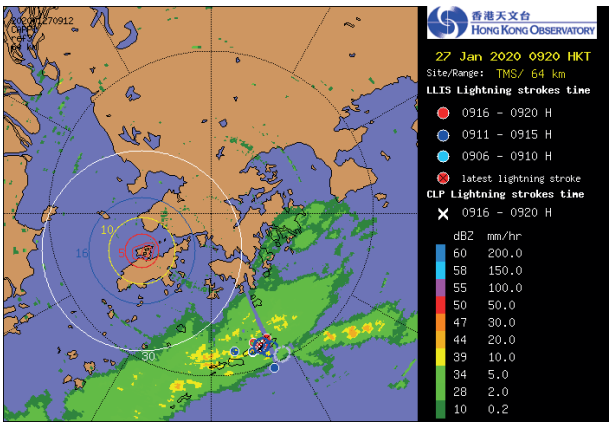

Fig. 4. Radar picture (from the S-band radar) and the associated lightning strikes (cloud-to-ground, with timing on the right).

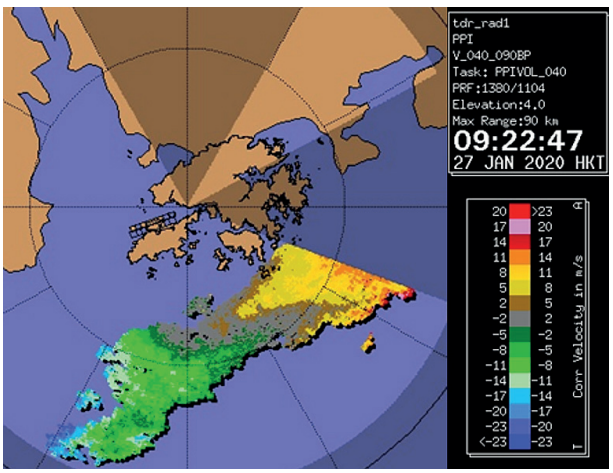

Fig. 5. Doppler velocity given by the terminal Doppler weather radar at the time of the thunderstorm.

at about 40-50 km to the southeast of Hong Kong (Fig. 4). Given the proximity of the radar echoes and lightning strikes near Hong Kong, thunder would likely be heard over the territory. This is consistent with the authors' observations.

A southwesterly flow of around 14 m s^{-1} was depicted in the radar echo of the C-band weather radar to the southeast of Hong Kong (Fig. 5). It also appeared there was a convergence between outbound and inbound flow at the location of the stronger radar echo. This mid-level convergence could be favorable to the development of the rain clouds.

From the hydrometeor classification by the S-band radar (Fig. 6), graupels (yellow) were found to be embedded in the extensive area of rain/wet snow/snow, which further supports the occurrence of lightning over that region of radar echo. The presence of graupels would likely lead to the occurrence of thunders and lightning due to their collisions.

Both cloud-to-cloud (i.e., intra-cloud) and cloud-to-ground lighting strikes were also registered by the global lightning network at roughly the same location, with peak current of over 50 kA (Fig. 7).

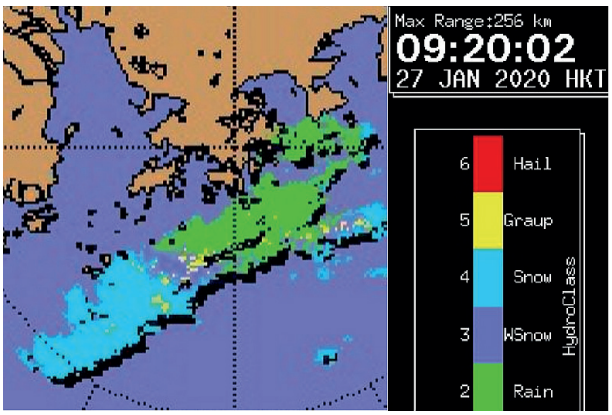

Fig. 6. Hydrometeor classification for the radar echo from the S-band radar at the time of the thunderstorm.

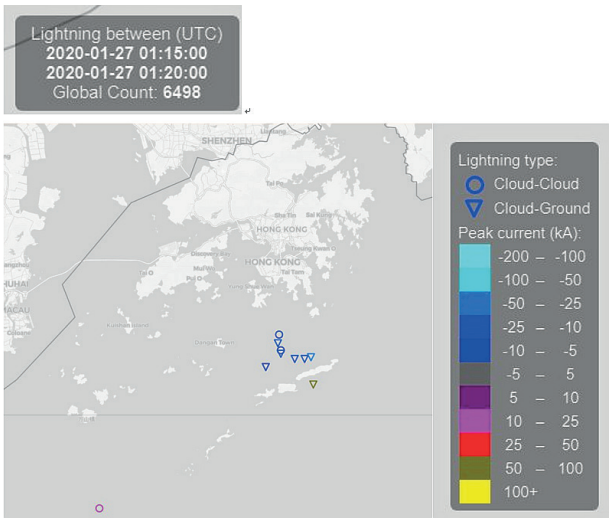

Fig. 7. Lighting locations as given by the global lightning location system. Descriptions of the shape and color of the symbols are shown on the right.

The observations of the global lightning network and the lightning strikes registered by LLIS are generally consistent with each other.

The thermodynamic conditions of the atmosphere were displayed in the radiosonde measurement at 00:00 UTC, January 27, 2020 (Fig. 8a). The atmosphere was moist between around 550 and 700 hPa. Below that, the atmosphere was rather dry and the K-index registered only 25 K. CAPE could not be calculated as there was a strong temperature inversion in the lower troposphere.

The microwave radiometer (Fig. 8b) also showed that, at about 01:20 UTC on January 27, the troposphere was rather dry at the level of about 2200 masl. CAPE was very small at only about 20 J kg^{-1}, and the K-index was about 18 K. The thermodynamic indicators in general did not favor the occurrence of deep convection.

The wind profiler (Fig. 9) showed that, at around 01:20 UTC on January 27 there appeared to be a westerly wave moving around that location at a height of about 2 to 3 km above the mean sea level. This wave was considered to be a major feature for triggering the convection.

In summary, from both the radar wind profiler and satellite images, the dynamic conditions suggested the occurrence of a deep convection, namely a, troughing flow in the lower troposphere and a westerly wave in the middle troposphere.

4. Performance of the Numerical Weather Prediction (NWP) model

We hereby inspect the AAMC-WRF model run initialized at 06:00 UTC on January 26, 2020, which would have been available to the forecasting bench around local evening time the day before the thunderstorm event took place. Figure 9a shows the simulated radar reflectivity in the vicinity of Hong Kong at a height of 5 km. It can be seen that a wave-like echo patch, with maximum intensity not exceeding 30 dBZ, was predicted to take place to the south of Hong Kong. While the shape of the simulated echo patch bears reasonable resemblance to the actual radar observations in terms of both shape and intensity, we can also notice some deficiencies. Firstly, the simulated echo patch did not extend far enough towards the northeast and therefore it did not cover the actual location where lightning was detected. From here, we shall proceed to inspect the cause of this flaw. Figure 9b shows the predicted cloud ice content (mixing ratio in g kg^{-1}) at the same altitude. The AAMC-WRF model was able to produce a southwest-northeast oriented band just to the south of Hong Kong, which corresponded to the observed cloud band on satellite images. Hence, the synoptic feature of the frontal cloud band was correctly positioned. Figure 9c shows the predicted graupel content (mixing ratio in g kg^{-1}), also at an altitude

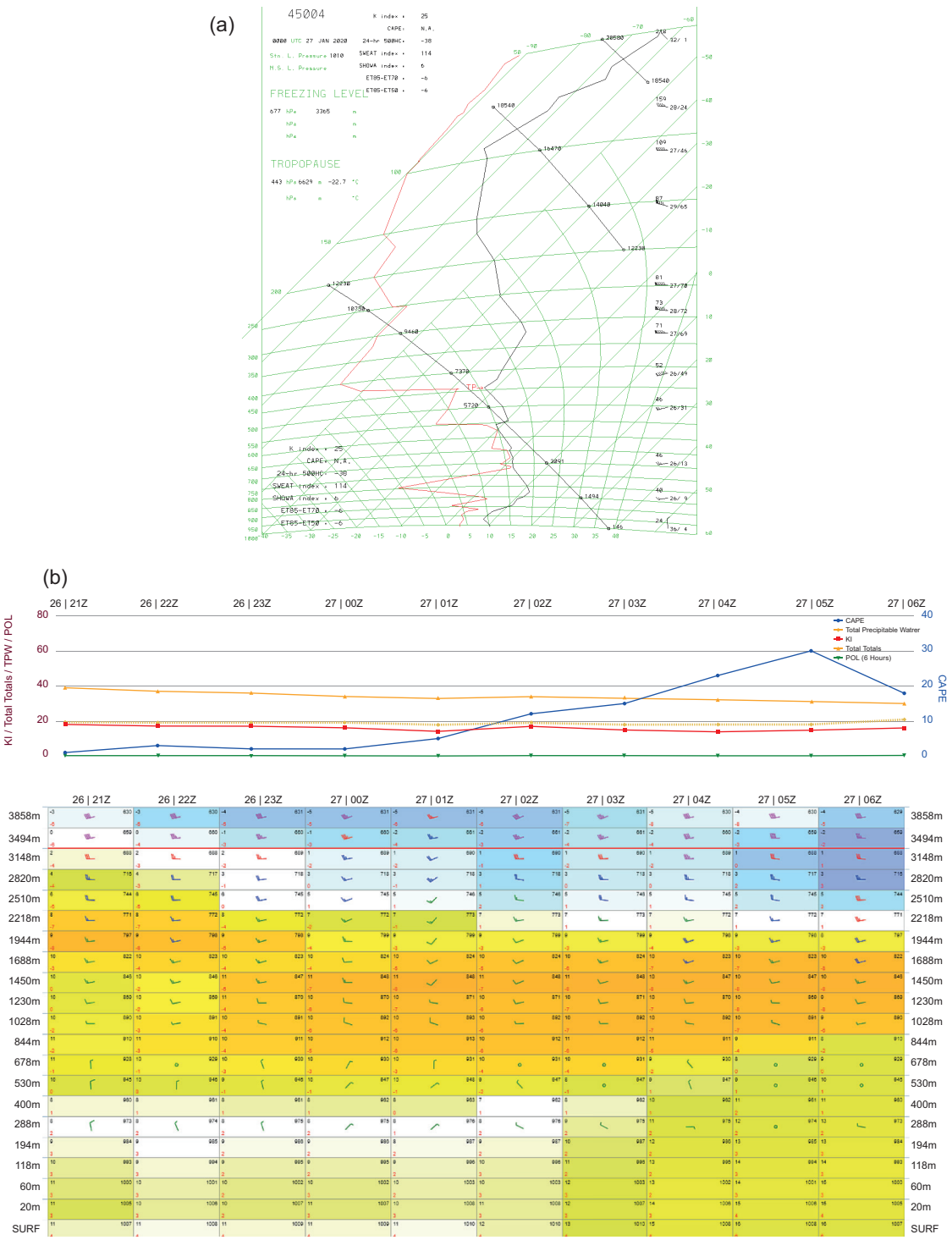

Fig. 8. (a) Hong Kong tephigram at 00:00 UTC on January 27 2020. (b) Humidity data from the microwave radiometer (color scale) and the time series of various instability indices. The grey column shows missing data from the wind.

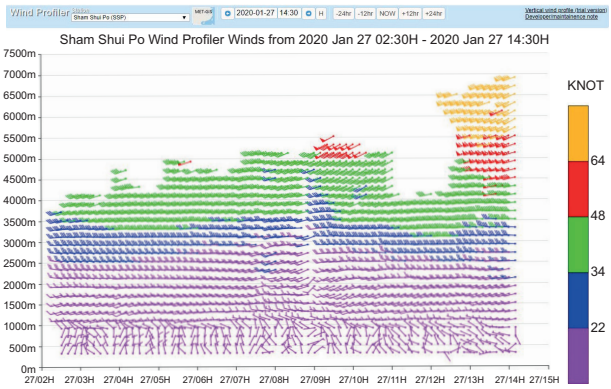

Fig. 9. Wind profiler data. The color scale shows wind speed in knots.

of 5 km. It can be seen that the model produced a concentrated region of graupel (peaking at about 0.1 g kg^{-1}) which is co-located with the model-predicted feature of radar reflectivity. While the occurrence of the model graupel was in line with the satellite-based analysis in section 3.2 and was also a favorable ingredient for lightning, the predicted spatial extent was too small to reproduce the full shape of the lightning-bearing echoes closest to Hong Kong.

Secondly, the simulated radar reflectivity feature took place at a very high altitude. This is why the 5-km layer was chosen in Figure 9, below which the predicted reflectivity values turn out to be very low. The upper-air winds and relative humidity around Hong Kong as predicted by the AAMC-WRF are

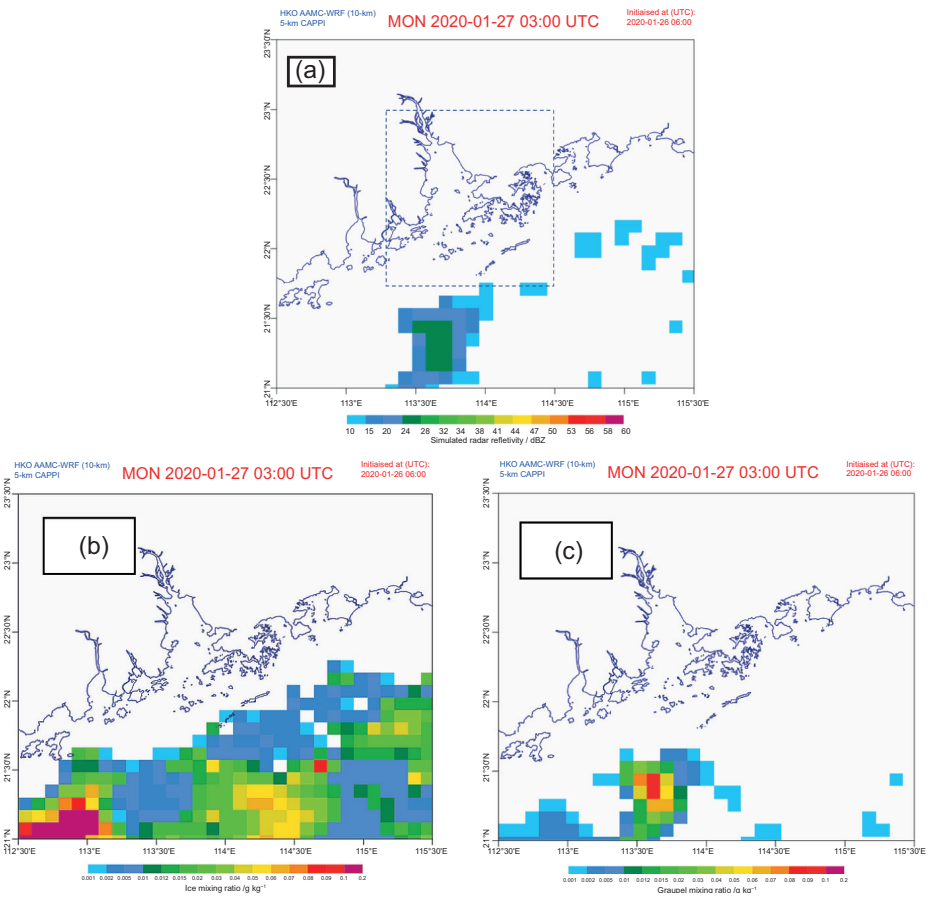

Fig. 10. Forecast meteorological fields at 5-km altitude by the AAMC-WRF model, taken from the real-time operational run initialized at 06:00 UTC on January 26, 2020. (a) Simulated radar reflectivity (the domain of Fig. 4 is given by a rectangle with broken line). (b) Cloud ice content. (c) Graupel content.

given in Figure 10. The top panels (left to right) depict the 500 and 700 hPa layers. The moist patches (in shades of blue) to the south of the coastline agree reasonably well with the observed cloud bands, while at 500 hPa there are signs of short waves to the south of Hong Kong. However, the bottom panels (850 and 925 hPa, left to right) show that the dry continental airflow near the bottom of the troposphere had penetrated too far in a southward direction, to the extent that the occurrence of hydrometeors and hence radar reflectivity in the model were stifled.

At the time of the thunderstorm event, the AAMC-WRF model only made use of conventional GTS observations for data assimilation. In Figures 11 and 12, we present simulation results from a re-run utilizing additional observation data. The re-run was initialized at 00:00 UTC, January 26 2020 with assimilation of Himawari-8 atmospheric motion vectors (AMV) on top of conventional GTS observations. Here the output at 02:00 UTC (i.e., 1 h earlier than that shown in Figs. 9 and 10) are shown, which are able to better match the actual timing of the thunderstorm event. By comparing Figures 9 and 11, it can immediately be seen that the re-run is able to better capture the proximity of the radar echoes to Hong Kong (the main echo band shifted northwards from below 21.5º N to around 22.0º N) with enhanced coverage of ice and graupel contents. By comparing Figures 10 and 12, we may attribute the

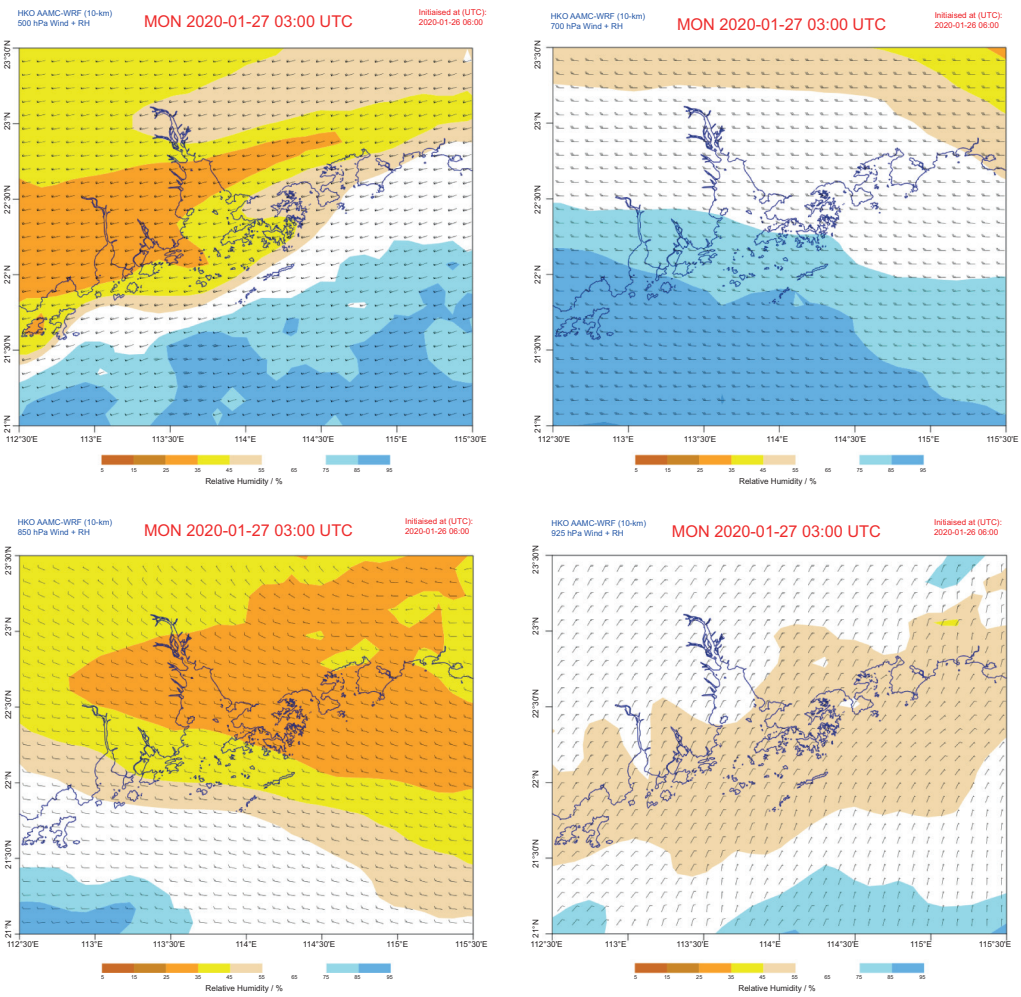

Fig. 11. Forecast upper-air winds and humidity fields by the AAMC-WRF model taken from the real-time operational run initialized at 06:00 UTC on January 26, 2020. Top row left to right: 500 and 700 hPa isobaric levels. Bottom row, left to right: 850 and 925 hPa isobaric levels.

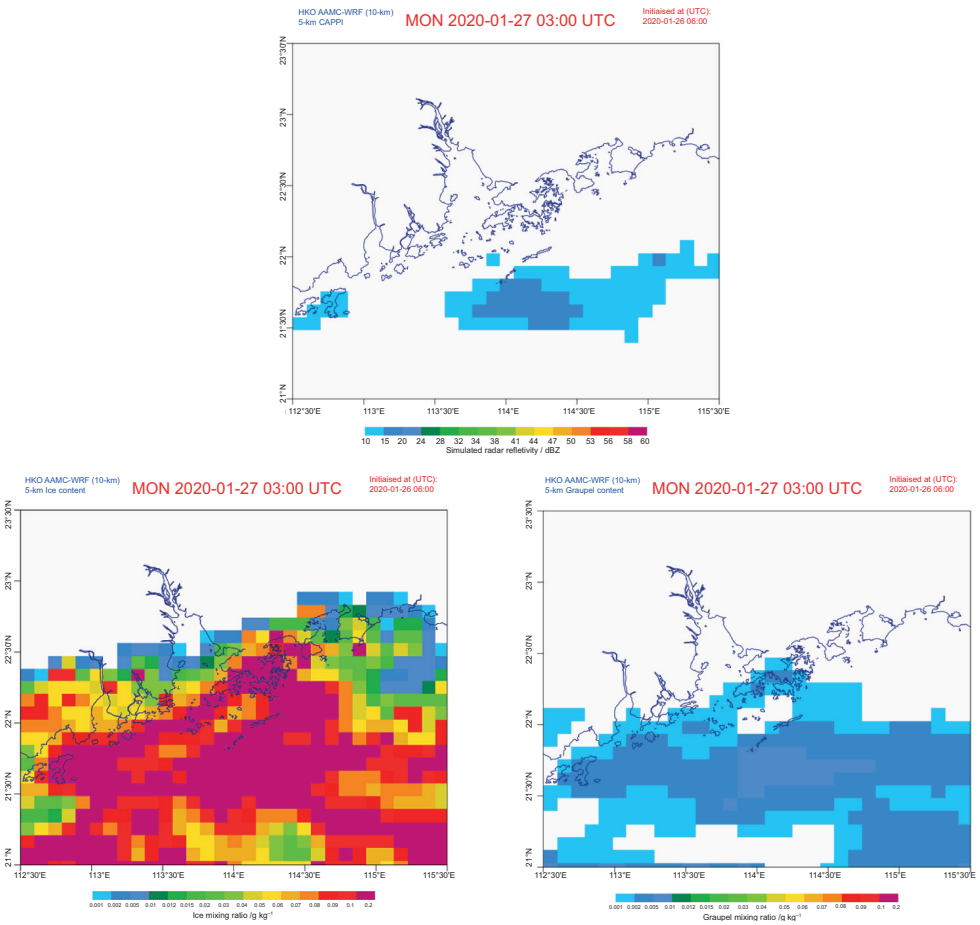

Fig. 12. Same as in Figure 9 but using the output from a re-run initialized at 00:00 UTC on January 26, 2020 and valid at 02:00 UTC on January 27.

differences to enhanced moisture at 500 and 700 hPa levels, especially over Hong Kong, which provides a more favorable environment for the development and maintenance of the simulated radar echoes closer to Hong Kong. Furthermore, we note from Figure 13 that in the re-run it has become possible to reproduce the simulated radar reflectivity at 3-km altitude around Hong Kong, which was not possible previously in the original real-time operational run (hence a 5-km altitude was chosen in Fig. 9).

5. Summary

A rare winter thunderstorm case in Hong Kong is documented in this paper. The convection was quite intense, as shown by the peak current of the lightning strike. The occurrence of thunder was also supported by weather radar observations. The thermodynamic conditions of the atmosphere did not appear to support deep convection; however, a troughing flow could be analyzed in the lower troposphere, and there appeared to be westerly waves in the middle troposphere. Such dynamic conditions are favorable for the occurrence of a convection. From the tephigram (Fig. 6a), the air parcel at about 1500 m may have been lifted to the upper troposphere for the convection to take place, which was a kind of elevated thunderstorm. In terms of mesoscale model prediction, the 10-km resolution AAMC-WRF model of HKO was able to indicate a wave-like, graupel-rich radar reflectivity region to the south of Hong Kong, bearing reasonable resemblance to the observed radar and satellite features since the evening before the event (i.e., lead time of 18-21 h). Nonetheless, the predicted

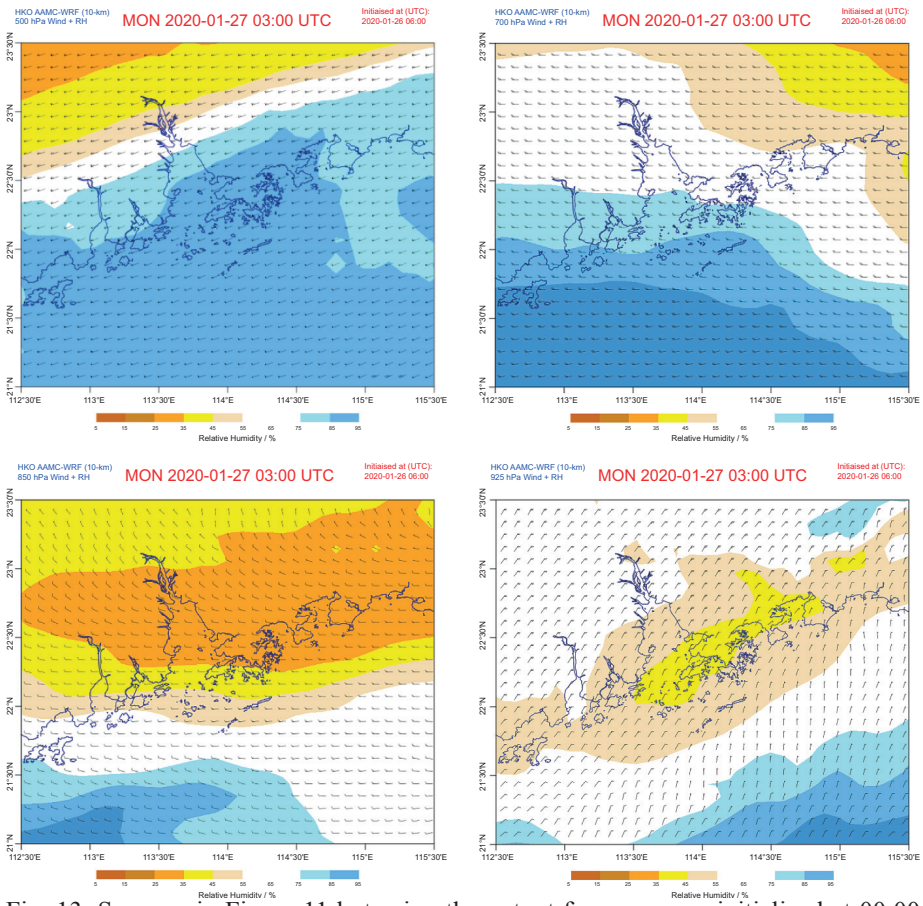

Fig. 13. Same as in Figure 11 but using the output from a re-run initialized at 00:00 UTC on January 26, 2020 and valid at 02:00 UTC on January 27.

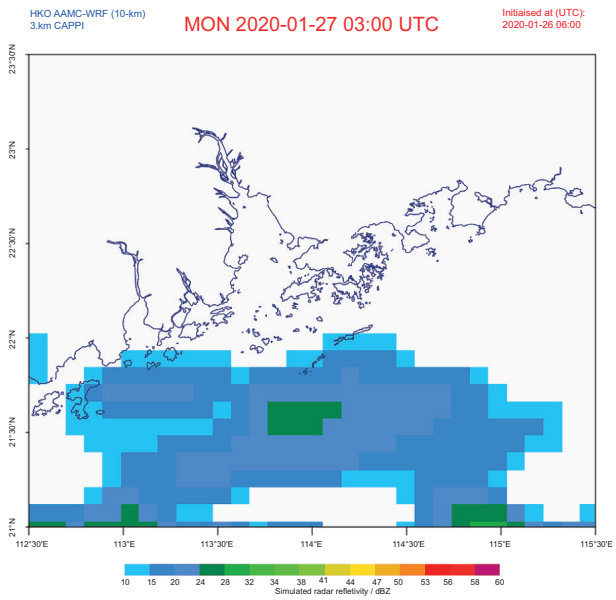

Fig. 14. Simulated radar reflectivity at 3-km altitude from a re-run initialized at 00:00 UTC on January 26, 2020 and valid at 02:00 UTC on January 27. In the real-time operational run (Figs. 9 and 10) no simulated reflectivity could be seen at that altitude.

reflectivity region occurred too high in altitude due to a deficiency of lower tropospheric moisture and did not extend far enough in the northeast direction to coincide with the actual lightning location, due to misplacement of the high graupel content region. The timing, location and vertical structure of the simulated reflectivity pattern could be improved through assimilation of additional upper-air observations in the form of Himawari-8 AMVs. It is hoped that this paper can be useful as reference for future forecasting of similar rare and unseasonal convection events at subtropical latitudes, and also highlight challenges in the analysis and modeling of such events.

References

Chan PW, Yeung KK. 2003. experimental extension of the measurement range of a boundary layer wind profiler to about 9 km. 12th Symposium on Meteorological Observations and Instrumentation, Long Beach, California, USA, February 10-13. Available at: https://www.hko.gov.hk/en/publica/reprint/files/r497.pdf

Chan PW. 2009. Performance and application of a multi-wavelength, ground-based microwave radiometer in intense convective weather. Meteorologische Zeitschrift 18: 253-265. https://doi.org/10.1127/0941-2948/2009/0375

Chan PW. 2010. The use of neural network retrieval for thermodynamic profiles of a ground-based microwave radiometer. In: 11th Specialist Meeting on Microwave Radiometry and Remote Sensing of the Environment, Washington, DC, USA, March 1-4. Available at: https://www.hko.gov.hk/en/publica/reprint/files/r891.pdf

Chan PW, Hon KK. 2011. Application of ground-based, multi-channel microwave radiometer in the nowcasting of intense convective weather through instability indices of the atmosphere. Meteorologische Zeitschrift 20: 431-440. https://doi.org/10.1127/0941-2948/2011/0276

Chiu YY, Lee OSM. 2019. Fine-scale comparison of regional and global lightning location data over the Pearl River Estuary region. 33rd Guangdong-Hong Kong-Macao Meteorological Technical Seminar, Hong Kong, March 6-8. Available at: https://www.hko.gov.hk/en/publica/reprint/files/r1358.pdf (English abstract only).

Derrien M, Le Gléau H. 2005. MSG/SEVIRI cloud mask and type from SAFNWC. International Journal of Remote Sensing 26 : 4707-4732. https://doi.org/10.1080/01431160500166128

Hon KK. 2018. Simulated satellite imagery at sub-kilometre resolution by the Hong Kong Observatory. Weather 73: 139-144. https://doi.org/10.1002/wea.3100

Hon KK. 2020. Tropical cyclone track prediction using a large-area WRF model at the Hong Kong Observatory. Tropical Cyclone Research and Review 9: 67-74. https://doi.org/10.1016/j.tcrr.2020.03.002

HKO. 2019. World Meteorological Organisation Regional Specialised Meteorological Centre for Nowcasting. Hong Kong Observatory. Available at: https://rsmc.hko.gov.hk/nowcast/

HKO. 2020. Number of days with thunderstorm in Hong Kong since 1947. Hong Kong Observatory. Available at: https://www.hko.gov.hk/en/cis/statistic/tsday_statistic.htm

Iacono MJ, Delamere JS, Mlawer EJ, Shephard MW, Clough SA, Collins WD. 2008. Radiative forcing by long-lived greenhouse gases: Calculations with the AER radiative transfer models. Journal of Geophysical Research 113: D13103. https://doi.org/10.1029/2008JD009944

Kong W, Chan YW. 2018. Rapid scan experiment of Doppler weather. 2018. Radar for monitoring rainstorms and tropical cyclones in Hong Kong. In: 10th European Conference on Radar in Meteorology and Hydrology (De Vos L, Leijnse H, Uijlenhoet R, Eds.). Ede-Wageningen, The Netherlands, July 1-6. https://doi.org/10.18174/454537

Lim K-SS, Hong S-Y. 2010. Development of an effective double-moment cloud microphysics scheme with prognostic cloud condensation nuclei (CCN) for weather and climate models. Monthly Weather Review 138: 1587-1612. https://doi.org/10.1175/2009MWR2968.1

Liu H, Chandrasekar V. 2000. Classification of hydrometeors based on polarimetric radar measurements: Development of fuzzy logic and neuro-fuzzy systems, and in situ verification. Journal of Atmospheric and Oceanic Technology 17: 140-164. https://doi.org/10.1175/1520-0426(2000)017<0140:COHBOP>2.0.CO;2

Lee OSM. 2018. Latest development of the lightning location network over the Pearl River estuary and data analysis related to tropical cyclone monitoring. In: WMO Technical Conference on Meteorological and Environmental Instruments and Methods of Observation, Amsterdam, The Netherlands, October 8-11. Available at: https://www.hko.gov.hk/en/publica/reprint/files/r1351.pdf

Murata H, Takahashi M, Kosaka Y. 2015. VIS and IR bands of Himawari-8/AHI compatible with those of MTSAT-2/Imager. Technical report No. 60. Meteorological Satellite Centre, Japan Meteorological Agency, Tokyo, Japan.

Shin HH, Hong S, Noh Y, Dudhia J. 2013. Derivation of turbulent kinetic energy from a first-order nonlocal planetary boundary layer parameterization. Journal of the Atmospheric Sciences 70: 1795-1805. https://doi.org/10.1175/JAS-D-12-0150.1

Skamarock WC, Klemp JB. 2007. A time-split nonhydrostatic atmospheric model for weather research and forecasting applications. Journal of Computational Physics 227: 3465-3485. https://doi.org/10.1016/j.jcp.2007.01.037

Tse SM, Hagio M, Maeda Y. 2019. Windshear detection by terminal Doppler weather radar during tropical cyclone Mujigae in 2015. Meteorological Applications 26: 620-631. https://doi.org/10.1002/met.1789

Zhang C, Wang Y, Hamilton K. 2011. Improved representation of boundary layer clouds over the Southeast Pacific in ARW-WRF using a modified Tiedtke cumulus parameterization scheme. Monthly Weather Review 139: 3489-3513. https://doi.org/10.1175/MWR-D-10-05091.1